Molecular dynamics simulations supporting the development of a continuum model of heat transport in nanowires

Igor Bejenari
Modeling and Artificial Intelligence
Fraunhofer IISB
Erlangen, Germany
igor.bejenari@iisb.fraunhofer.de

Alexander Burenkov
Modeling and Artificial Intelligence
Fraunhofer IISB
Erlangen, Germany
Alex.Burenkov@iisb-extern.fraunhofer.de

Peter Pichler
Modeling and Artificial Intelligence
Fraunhofer IISB,
Chair of Electron Devices
University of Erlangen-Nuremberg
Erlangen, Germany
Peter.Pichler@iisb.fraunhofer.de

Ioannis Deretzis
Institute for Microelectronics and Microsystems
Physics and Matter Technologies Department of CNR
Catania, Italy
Ioannis.Deretzis@imm.cnr.it

Alberto Sciuto
Institute for Microelectronics and Microsystems
Physics and Matter Technologies Department of CNR
Department of Physics and Astronomy University of Catania
Catania, Italy
Alberto.Sciuto@imm.cnr.it

Antonino La Magna
Institute for Microelectronics and Microsystems
Physics and Matter Technologies Department of CNR
Catania, Italy
Antonino.LaMagna@imm.cnr.it

***Abstract*—We establish a suitable methodology for Molecular Dynamics (MD) simulations to provide reliable data for the development of continuum model extensions of Fourier's law, which reproduce effects arising from phonon confinement and interface scattering. This continuum approach for thermal transport is required for TCAD tools dedicated to nanoscaled electron device simulations.**

Keywords—nanowire, thermal transport, molecular dynamics, continuum approach

I. Introduction

To save computational resources, calculation of thermal transport in TCAD tools dedicated to electron devices is usually based on continuum approaches. For nanoscale devices, proper extensions of Fourier's law have to be implemented in continuum models to reproduce effects arising from phonon confinement and interface scattering. To provide reliable data for the development of such model extensions, a suitable methodology for Molecular Dynamics (MD) simulations has been developed. It is based on an innovative combination of heat sources and Langevin thermostats applied to silicon nanorods with silicon dioxide caps that allows a validation of the suggested MD model by comparison with the results of previous work as well as a direct comparison of MD simulations with the results of continuum simulations based on equivalent heating and boundary conditions. Our work is motivated by the development of a continuum model for the simulation of the laser annealing of silicon-based gate-all-around nanowire electron devices. In such systems, during laser annealing, the photon energy is mainly absorbed in the silicon because the silicon dioxide is transparent for the light used in laser annealing. Besides, because the diameter of the silicon nanowires is small in comparison to the absorption length of the laser light, a nearly uniform heating of the silicon nanowires is expected. Therefore, we focus here on the case of a uniformly distributed heat source within a silicon nanowire covered by silicon dioxide and consider the heat transport along the nanowire axis.

II. Methodology

We consider axial heat transfer along Si nanowires heated uniformly with a power of $\dot{Q}_{hot} = dQ/dt = 15$ eV/ps (Q is the heating energy) with the heat being dissipated through the end lids coated by amorphous SiO_2 layers as shown in Fig.1. This structure design enables a full characterization of the axial heat transfer including heat transport through the Si/SiO_2 interface, which is required for the calibration of a continuum model of heat transport along the silicon nanowire axis.

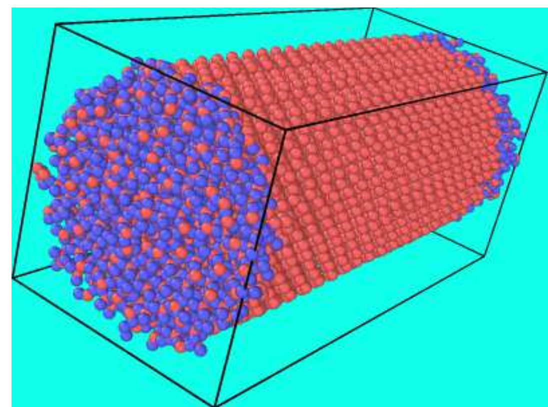

Fig. 1. Atomic arrangement consisting of 13748 atoms for the MD modelling of a 10-nm-long cylindrical Si nanowire with a diameter of 5.2 nm and with end lids coated by 1-nm-thick amorphous SiO_2 layers. The figure was created by using OVITO [1].

Exploiting the open source simulation tool LAMMPS [2], stable version (3 Mar 2020), Non-Equilibrium Molecular Dynamics (NEMD) simulations were performed using Tersoff potentials [3]. The atomic structure of the amorphous

This is the post-print version of the original article I. Bejenari, A. Burenkov, P. Pichler, I. Deretzis, A. Sciuto, A. La Magna: Molecular Dynamics Simulations Supporting the Development of a Continuum Model of Heat Transport in Nanowires, 2021 27th International Workshop on Thermal Investigations of ICs and Systems (THERMINIC), IEEE, 194-199 (2021)
DOI: 10.1109/THERMINIC52472.2021.9626512

©2021 IEEE

silicon dioxide material was simulated by a heating of crystalline SiO_2 above the melting point, followed by a rapid cooling. Periodic boundary conditions were set at the boundaries of the MD simulation box, indicated by black lines in Fig.1. In our previous work [4], similar structures with a heat source in the middle and heat sinks at the periphery have been validated already against literature data [5, 6]. Recently, new experimental studies of temperature profiles along heated Al and GaP nanowires have been performed using scanning thermal microscopy and Raman thermometry [7, 8]. Similar experiments could also be used to validate the NEMD simulations of temperature profiles in heated Si nanowires.

Unfortunately, the formulation of the heat transport by means of the heat sources and heat sinks, which is rather common in MD simulations, leads to numerical problems and ill-defined numerical solutions in continuum approaches [9, 10]. The continuum model that we envisage to calibrate using these MD simulations employs extended heat sources inside of the simulation domain and Dirichlet boundary conditions at the borders of the simulation domain acting as heat sink.

III. Comparison of MD Simulations with Continuum Approaches

To allow a direct comparison of MD simulations with continuum model simulations and so to establish a continuum model calibration procedure by this comparison, we consider here a NEMD set-up in which Langevin thermostats are used as heat sinks. Specifically, the thermostats are located in the outermost 4 Å of the SiO_2 lids to establish there the external cooling temperature in analogy to the temperature of the Dirichlet boundary conditions in the continuum model.

To verify the MD model of this paper with Langevin thermostats we compare it with the model of our previous work [4] which excluded thermostats and used heat sources and sinks only. Figs 2 and 3 show the temperature profiles along the silicon nanowire axis calculated by our previous MD model and the new MD model for targeted average temperatures of 300 K, respectively. In both MD simulations, steady state in the temperature distribution has been reached within the simulation time of 12 ns. Both MD models provide similar temperature distributions along uniformly heated Si nanowires when the heat is released through the nanowire end lids coated by amorphous SiO_2 layers with different thicknesses. Slight differences between corresponding curve shapes are related to statistics and the different thermal boundary conditions associated with the use of heat sinks and thermostats. In the new simulation setup, the target average temperature had to be established by manually setting the temperature of the thermostat. This way, the mean temperature could be determined within about 10 K with reasonable effort. The resulting rigid temperature shifts between corresponding curves in Figs 2 and 3 are irrelevant for the further analysis.

Fig. 4 illustrates a result of the simulation of the thermal transport in the same nanowire with the same heating and thermal boundary conditions as in the MD simulations of Fig. 3. In the continuum model which takes into consideration phonon transport corrections, separate temperature fields (e.g. T_1 and T_2) in the regions with different materials are ruled by a Fourier law heat equation with the corresponding bulk conductivity values for these materials (e.g. κ_1 and κ_2). Standard continuity conditions (T_1=T_2) at the interface between different materials are replaced by jump conditions (see Eq. 5 of Ref. [9]), ruled by the local functional $(\kappa_1/\lambda_1 + \kappa_2/\lambda_2)|_\Gamma$ at the Γ interface location, where λ_i is the average phonon mean free path in the i-th-material. We notice that when the conductivity values for the materials are fixed, the interface temperature discontinuity depends on the estimates of effective λ_i. A thermal conductivity value of 2.1 W/K/m was taken for the bulk amorphous SiO_2 from MD simulations reported in the literature [11], while the (temperature-dependent) experimental value of κ was used for bulk Si [9].

The temperature distribution in Fig. 4 obtained by the continuum model reproduces the most essential features of the MD simulation results presented in Figs 2 and 3.

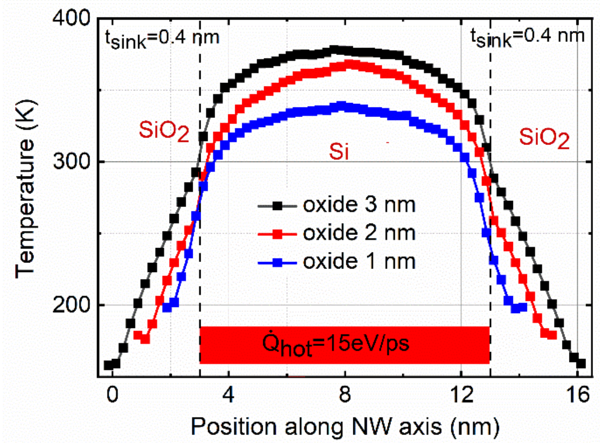

Fig. 2. Temperature distribution along the axis of the cylindrical nanowire with a radius r_{NW} of 2.6 nm obtained in our previous NEMD model for an average temperature of about 300 K in steady-state. Two heat sinks with thicknesses t_{sink} and powers of -7.5 eV/ps each are set in outer parts of the the a-SiO_2 layers on the Si nanowire tip.

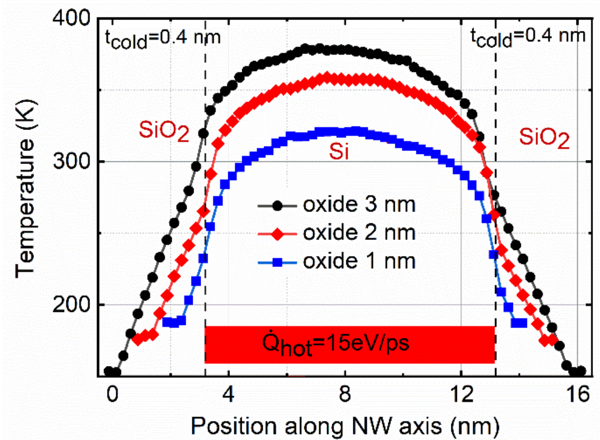

Fig. 3. Temperature distribution along the axis of the cylindrical nanowire with a radius of 2.6 nm obtained in the current NEMD model. The lowest temperatures in the thermostat-controlled regions are 187, 175, and 153 K for average nanowire temperatures of 280, 295, and 293 K in steady-state for the a-SiO_2 layers with thicknesses of 1, 2, and 3 nm, respectively. The thickness, t_{cold}, of each of the thermostatically controled regions in the outer parts of the a-SiO_2 layers is 0.4 nm.

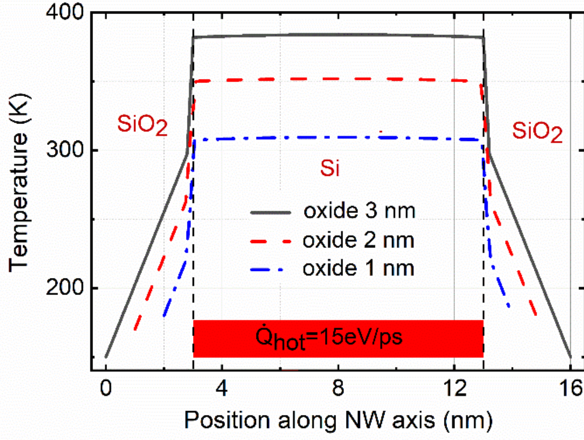

Fig. 4. Temperature distribution along the axis of the cylindrical Si nanowires with amorphous SiO_2 layers of 1, 2 and 3 nm thickness on the nanowire tips obtained in the continuum model. Model parameters: $\lambda_{Si} = 59.6\ nm$ and λ_{SiO_2} =30.2 nm.

Specifically, the maximum temperature and the difference between the maximum and cooling temperatures are well reproduced.

The distribution of the temperature inside of the silicon nanowire in the continuum model is significantly flatter than in the MD simulations. This can be explained by the usage of the bulk values for the thermal conductivity of silicon, which is about κ =140 W/(Km) at room temperature.

IV. MD Simulation Results for Elevated Temperatures

Laser annealing is usually carried out at high temperatures up to melting point, which happens, for example, at 1687 K for silicon. With the aim to obtain thermal data for the modeling of the heat transfer in nanostructures at such high temperatures, MD simulations were performed for mean temperatures of 800 K and 1300 K.

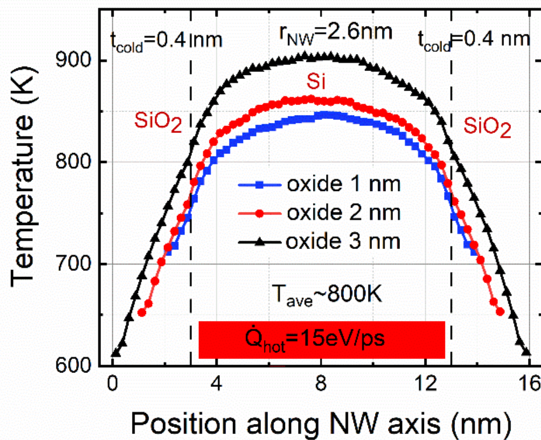

Fig. 5. Temperature distribution along the axis of the cylindrical Si nanowires with amorphous SiO_2 layers of 1, 2 and 3 nm thickness on the nanowire tips obtained with the MD model of this work for average temperatures of 803, 793, and 805 K corresponding to different oxide thicknesses.

Fig. 5 shows the temperature distribution in the silicon nanowire and the oxide lids as shown in Fig. 1 for an average sample temperature of 800 K. The average temperature was calculated from the average kinetic energy of all atoms in the system.

Fig. 6 shows the same temperature distributions as in Fig. 5 but for an average temperature of 1300 K. The difference between the temperature in the middle of nanowire and the temperature of the thermostaticall controlled regions increases with an increase of the average temperature.

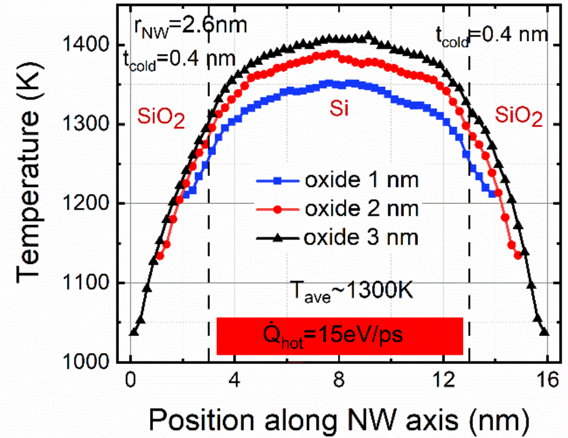

Fig. 6. Temperature distribution along the axis of the cylindrical Si nanowires with amorphous SiO_2 layers of 1, 2 and 3 nm thickness on the nanowire tips obtained with the MD model of this work for average temperatures of 1312, 1303, and 1290 K corresponding to different oxide thicknesses.

Fig.7 shows reduced radial temperature distributions in a nanowire slice perpendicular to the nanowire axis with a thickness of 2 nm in the middle of the Si nanowire shown in Fig. 1 for values of the average nanowire temperature of 290, 800, and 1300 K. The temperature at the nanowire surface at the radius of 2.6 nm tends to decrease by approximately 5% at 290 K. This effect diminishes with increasing average temperature. In contrast to predictions based on the classical heat transfer theory, the temperature distribution along the nanowire diameter is not quite uniform.

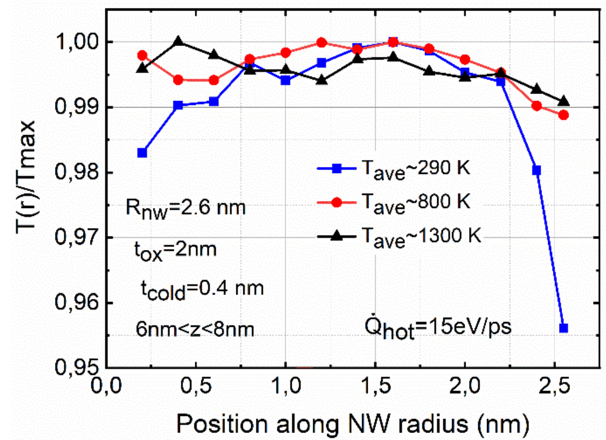

Fig. 7. Reduced radial temperature distribution in an Si nanowire slice with a thickness of 2 nm in the middle of nanowire for three average temperatures T_{ave}.

However, the temperature variations are less than 1% and are not expected to significantly impact the accuracy of the longitudinal heat transport parameters.

In the next section, we describe a methodology for extracting parameters used in empirical continuum models, such as thermal resistance and thermal conductivity of the SiO_2/Si nanowires from NEMD simulations.

V. Parameter Extraction from MD Simulations

To extract effective thermal parameters suitable for usage in empirical continuum models, we analyze in the following the derivatives of the temperature distributions obtained from MD simulations. Fig. 8 depicts the spatial derivative of the temperature along the nanowire for different values of the oxide thickness and an average temperature of 290 K. In the Langevin thermostats, the derivative of the temperature tends to zero because of the fixed temperature. There are two distinct spikes located at the SiO_2/Si interfaces.

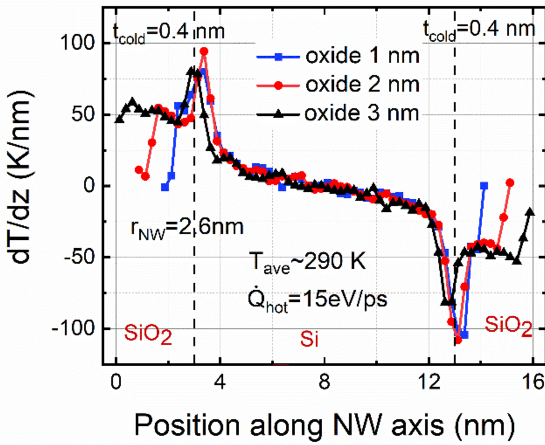

Fig. 8. Temperature derivative distribution along the axis of the cylindrical Si nanowires with amorphous SiO_2 layers of 1, 2 and 3 nm on the nanowire tips obtained with the MD model of this work for an average temperature of 290 K.

In the oxide layers between the Langevin thermostats and the interface to the heated nanowire, the temperature derivative in steady-state is approximately constant in accordance with classical Fourier's law

$$q = -\kappa_{ox} \frac{dT}{dz} \quad (1)$$

Therein, q is the constant local heat flux density between the Langevin thermostats and the heat source, κ_{ox} is the thermal conductivity in the oxide, and z is the coordinate along which the heat flux is studied. In our symmetrical simulation setup, q is equal to 0.057 W/μm^2. Taking the constant derivative dT/dz in silicon dioxide from Fig. 8 and using (1), we obtain the effective thermal conductivity κ_{ox} of the silicon dioxide layers at 290 K. For all values of the oxide thickness, the thermal conductivity of SiO_2 at 290 K was found to be 1.2 ± 0.08 W·K^{-1}·m^{-1}.

A detailed look at the spatial derivative of the temperature reveals that the assumption of a constant temperature gradient in the oxide is only approximate. Consequently, the application of Fourier's law must be questioned. Below, an alternative approach is used to evaluate the thermal resistance of the oxide layers which avoids the limiting assumptions of this first analysis.

Inside the silicon nanowire at a distance of at least 1 nm from each SiO_2/Si interface, the temperature derivative dependents approximately linearly (see Fig. 8) on the space coordinate along which the heat transport is studied. The small MD-inherent temperature fluctuations along the radius of the nanowire in Fig. 7 indicate rather negligible radial temperature gradient until shortly before the surface. For the axial heat transfer, the classical steady-state heat equation taking into account the uniformly distributed heat source with a power of $\dot{Q}_{hot} = 15$ eV/ps inside the nanowire with a volume of V_{Si} reads:

$$-\kappa_{Si} \frac{d^2T}{dz^2} = \frac{\dot{Q}_{hot}}{V_{Si}} \quad (2)$$

Integrating both sides of (2), we obtain a classical expression for the derivative of the temperature along the axis of the Si nanowire

$$\frac{dT}{dz} = -\frac{\dot{Q}_{hot}}{\kappa_{Si} V_{Si}} z + constant \quad (3)$$

Using (3), we estimate the thermal conductivity κ in the Si nanowires from the temperature derivatives obtained from our MD simulations as shown for 290 K average temperature in Fig. 8. The results are listed in Table I. The standard deviations shown in Table I result from the evaluation of the temperature distributions in nanowires with oxide layers of different thicknesses at the tips.

TABLE I. Effective Thermal Conductivity in the Si Part of the SiO_2/Si Nanowire Extracted from Fig. 8 Using the Classical Heat Equation

T_{ave} (K)	κ_{Si} (W·K^{-1}·m^{-1})
290	3.21 ± 0.07
800	2.32 ± 0.04
1300	2.18 ± 0.03

The values of the thermal conductivity κ extracted from the MD simulations of the axial thermal transport in the nanowires considered are significantly lower than the values of κ for bulk silicon, but they are also significantly higher than the values for radial transport in silicon nanowires with localized heat sources [4]. Such intermediate values of the thermal conductivity for silicon in nanowires with a limited length can be understood in terms of the concepts for different regimes of thermal transport in nanoscaled semiconductor and insulator structures [12].

One of the most important measurable parameters used to characterize heat transfer is thermal resistance. The difference between the maximum temperature and the temperature of a cooler defines in steady state the effective thermal resistance between the element that is heated and the cooler system consisting of two thermostats in our case.

$$R_{th} = (T_{max} - T_{cool})/\dot{Q}_{hot} \quad (4)$$

The one-sided thermal resistance between (strictly the respective half of) the nanowire and one of the cooling thermostat has twice the value value of R_{th} defined by (4):

$$R_{th1} = 2R_{th} \quad (5)$$

Eq. 5 follows from the fact that our MD simulation sample has a mirror symmetry with respect to the plane in the middle of the nanowire and perpendicular to the nanowire axis, so that the two equivalent cooler thermostats work as in a parallel resistance network.

From the temperature distributions obtained by MD simulations, taking into account the known power of the heat source distributed inside of the silicon nanowire we calculated the one-side thermal resistance of the silicon nanowire covered by oxide layers of different thickness. The results are presented in Fig. 9.

When comparing these results to the axial thermal resistances obtained in our previous work [4] we note that these were values obtained for a two-sided configuration, i.e. half of those shown in Fig. 9. Considering also the smaller effective oxide thickness in the current set-up, we note a very good agreement.

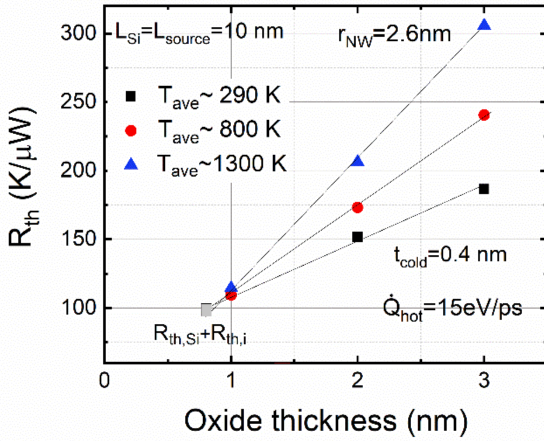

Fig. 9. One-sided thermal resistance between a uniformly heated silicon nanowire and a cooler thermostat on the external boundary of the oxide layer covering the nanowire tip for three average temperatures T_{ave}. $R_{th,Si}$ is the thermal resistance of the Si part of the nanowire, $R_{th,i}$ is the interfacial thermal resistance

The one-sided thermal resistance R_{th1} is composed of three components, namely the thermal resistance of the oxide layer $R_{th,ox}$, the interfacial thermal resistance $R_{th,i}$, and the one-sided thermal resistance of the Si part of the nanowire $R_{th,Si}$. The relation between these components is given by the following expression

$$R_{th1} = R_{th,ox} + R_{th,i} + R_{th,Si} \tag{6}$$

where $R_{th,ox}$ can be expressed by means of the thermal conductivity κ_{ox} of the silicon dioxide layer by

$$R_{th,ox} = \frac{L_{ox}}{A\kappa_{ox}} \tag{7}$$

Therein, A is the area of the nanowire cross section, and L_{ox} the respective layer thickness.

The thermal resistance of the oxide is mainly determined by the heat transfer via the atoms located between the Langevin thermostat with its thickness of 0.4 nm and the interface to the silicon. From the MD simulations we observe a linear dependence between the thermal resistance and the oxide thickness. The different slopes can be interpreted as a change of the thermal conductivity of the oxide with temperature. When only L_{ox} is varied, (5) with $R_{th,ox}$ from (6) reduces to

$$\Delta R_{th} = \Delta R_{th,ox} = \frac{\Delta L_{ox}}{A\kappa_{ox}} \tag{8}$$

Thus, the oxide thermal conductivity can be expressed as

$$\kappa_{ox} = \frac{1}{A}\frac{\Delta L_{ox}}{\Delta R_{th}} \tag{9}$$

Table II shows the mean effective thermal conductivity of thin amorphous oxide layers obtained from the evaluation of the results shown in Fig. 9 by (9). The strictly linear relationship between $\Delta R_{th,ox}$ and ΔL_{ox} indicates that the thermal conductivity of the oxide layers does not significantly depend on thickness. At 290 K, the value obtained for the thermal conductivity corresponds well to the result of the simpler analysis presented above. At higher temperatures, a significant reduction of the thermal conductivity can be observed.

TABLE II. EFFECTIVE THERMAL CONDUCTIVITY OF SiO_2 LAYERS WITH THICKNESSES OF 1, 2, AND 3 NM EXTRACTED FROM FIG. 9

T_{ave} (K)	κ_{ox} (W·K^{-1}·m^{-1})
290	1.23
800	0.717
1300	0.492

At the interfaces between the silicon dioxide layers and the silicon nanowire, the temperature derivative shows prominent spikes. Such a temperature behavior is due to phonon reflections at the interface and does not follow immediately from the Fourier equation. Continuum models simulate this effect by a temperature jump at the interface. It means that derivative of the temperature has ideally the shape of a delta function multiplied by a constant which is equal to the temperature jump at the interface. The integral over the derivative peak in the MD simulations must be equal to the temperature jump in the continuum model to reproduce the same temperature distribution in both models. Accordingly, the temperature jump can be extracted from the results of the MD simulation by integrating the peak in the temperature derivative versus space coordinate to obtain the interface resistance for the continuum model. The spikes in Fig. 8 are asymmetrically located around the interface plane. About 30 % of the spike is located in the SiO_2 material, i.e., at a distance less than 0.3 nm from the interface plane, and the other 70 % of the spike is in the Si material, i.e., at a distance less than 0.7 nm from the opposite site of the interface plane. From Figs. 3, 5 and 6, we obtain the variation of the temperature ΔT across the interface in the appropriate localization interval of the spikes, and are able to calculate the corresponding interfacial thermal resistance. At 800 and 1300 K, the interfaces were found the spikes to extend approximately over a similar interfacial thickness of 1 nm. The results of the evaluation of the near-interface temperature behavior are listed in Table III.

At room temperature, the product of the interfacial thermal resistance and the nanowire area, $R_{th,i}A$ =1.33×10^{-9} m^{2}K/W, is consistent with the value of 1.2×10^{-9} m^{2}K/W obtained previously for the heterostructure of silicon/amorphous silicon dioxide with a strong coupling strength through MD simulation [6]. With an increase in temperature from 290 K to

800 K, the derivative and the corresponding temperature jump at the SiO_2/Si interface decrease. With a further increase in the average temperature to 1300 K, the derivative and the temperature jump do not change significantly.

TABLE III. EFFECTIVE INTERFACIAL THERMAL RESISTANCE AND TEMPERATURE VARIATION IN THE INTERFACE REGION WITH A THICKNESS OF 1 NM AND CROSS-SECTION AREA OF A=21 NM^2 EXTRACTED FROM NEAR-INTERFACE TEMPERATURE DISTRIBUTIONS

T_{ave} (K)	ΔT (K)	$R_{th,i}$, (K·µW^{-1})
290	75 ± 9	62 ± 7
800	61 ± 1	50 ± 1.3
1300	60 ± 3	50 ± 2.7

To validate the determination of the thermal resistance of the interface, we have developed an alternative method to estimate the interfacial thermal resistance from an interpolation of (6) to a vanishing oxide thicknesses. As already indicated above, the relevant part of the oxide layer extends from outside of the Langevin thermostat with its thickness of 0.4 nm to the interface region which starts at 290 K about 0.3 nm before the geometrical interface. Hence, the oxide layer contributing to $R_{th,ox}$ effectively vanishes for a physical oxide thickness of 0.7 nm and the one-sided thermal resistance R_{th1} becomes equal to $R_{th,Si}$+$R_{th,i}$. The respective point has been marked by a grey square in Fig. 9 and denoted by $R_{th,Si}$+$R_{th,i}$. Now, if $R_{th,Si}$ is known, the thermal interface resistance $R_{th,i}$ can immediately be calculated from the known sum of $R_{th,Si}$+$R_{th,i}$.

For the calculation of the temperature resistance of the nanowire silicon part, let us consider the temperature difference $T_{max} - T_{min}$ in the silicon part of the nanowire which can be obtained from a further spatial integration of (3)

$$T_{max} - T_{min} = \frac{\dot{Q}_{hot}}{2\,\kappa\,V_{Si}}\left(z_0 - \frac{L}{2}\right)^2 \quad (10)$$

Therein, z_0 is the position where the interface region ends in the silicon nanorod (0.7 nm below the silicon surface) and at which the minimum temperature T_{min} is defined. The maximum temperature T_{max}, on the other hand, will be found in the middle (L/2) of the nanowire. The one-sided thermal resistance of one half of the silicon part of the nanowire then reads:

$$R_{th,Si} = \frac{2(T_{max}-T_{min})}{\dot{Q}_{hot}} = \frac{1}{\kappa_{Si}\,V_{Si}}\left(z_0 - \frac{L}{2}\right)^2 \quad (11)$$

where the thermal conductivity κ_{Si} of Si can be taken from Table I. The values for the one-side thermal resistance of the silicon part of the nanowires $R_{th,Si}$ calculated from (11), the extrapolated values for $R_{th,Si}$+$R_{th,i}$, and the extracted values for the effective interface thermal resistance $R_{th,i}$ are listed in Table IV.

TABLE IV. EFFECTIVE INTERFACIAL THERMAL RESISTANCE $R_{TH,I}$ OF SiO_2/ SI INTERFACE EXTRACTED FROM FIG. 9 AND THERMAL RESISTANCE OF SI.

T_{ave} (K)	R_{thSi} (K·µW^{-1})	$R_{th,Si}$+ $R_{th,i}$ (K·µW^{-1})	$R_{th,i}$ (K·µW^{-1})
290	31	100	69
800	44	89	45
1300	46	85	39

Considering the completely different approaches, we find a good agreement with the results in Table III.

VI. CONCLUSIONS

We have developed a simulation set-up for the characterization of thermal properties of nanoscaled silicon nanowires that can be used equivalently in both molecular dynamics and continuum simulations. With its help, it is possible to provide relevant data for the development and calibration of empirical TCAD continuum models suitable for nanoscaled electron devices. Our MD simulations indicate that the assumption of a temperature jump at the ideal Si/SiO_2 interface is an oversimplification. Instead, we find an interfacial layer with a small width of about 1 nm at 290 K in which the temperature gradient between two different materials exhibits a spike-like feature. The model parameters, such as the effective width of interfacial layer and the temperature difference across it, the interfacial thermal resistance, and the thermal conductivities of the silicon and silicon dioxide materials were estimated from the NEMD simulations.

ACKNOWLEDGMENT

The research leading to these results has received funding from the European Union's Horizon 2020 research and innovation programme under grant agreement No. 871813 MUNDFAB.

REFERENCES

[1] A. Stukowski, "Visualization and analysis of atomistic simulation data with OVITO–the Open Visualization Tool," Modelling Simul. Mater. Sci. Eng. vol. 18, pp. 015012(1-7), 2010.

[2] S. Plimpton, "Fast parallel algorithms for short-range molecular dynamics," J. Comp. Phys. vol. 117, pp. 1-19, March 1995; http://lammps.sandia.gov

[3] S Munetoh, T. Motooka, K. Moriguchi, and A. Shintani, "Interatomic potential for Si-O systems using Tersoff parameterization," Comput. Materials Sci., vol. 39, pp. 334-339, 2007.

[4] I. Bejenari, A. Burenkov, P. Pichler, I. Deretzis and A. La Magna, "Molecular dynamics modeling of the radial heat transfer from silicon nanowires," SISPAD 2020, Kobe, Japan, 2020, Piscataway: IEEE pp. 67-70.

[5] S. G. Volz, G. Chen, "Molecular dynamics simulation of thermal conductivity of silicon nanowires," Applied Physics Letters vol. 75 (14), pp. 2056-2058, October 1999.

[6] H. Gu, J. Wang, X. Wei, H. Wang and Z. Li, "Thermal conductivity and interfacial thermal resistance in the heterostructure of silicon/amorphous silicon dioxide the strain and temperature effect," Nanotechnology vol. 31, pp. 505703 (1-12), 2020.

[7] Daniel Vakulov, Subash Gireesan, Milo Y. Swinkels et al., "Ballistic phonons in ultrathin nanowires," Nano Letters vol. 20, pp. 2703-2709, 2020.

[8] N. Gächter, F. Könemann, M. Sistani et al., "Spatially resolved thermoelectric effects in operando semiconductor–metal nanowire heterostructures, ".Nanoscale vol. 12, pp. 20590–20597, 2020.

[9] A. Sciuto, I. Deretzis, G. Fisicaro et al. "Phononic transport and simulations of annealing processes in nanometric complex structures" Physical Review Materials vol. 4, pp. 056 007(1-6), 2020.

[10] A. Sciuto, I. Deretzis, G. Fisicaro et al., "Advanced simulations on laser annealing: explosive crystallization and phonon transport corrections," 2020 International Conference on Simulation of Semiconductor Processes and Devices (SISPAD), Kobe, Japan, 2020, pp. 71-74.

[11] J. M. Larkin and A. J. H. McGaughey, "Thermal conductivity accumulation in amorphous silica and amorphous silicon," Phys. Rev. B vol. 89, pp. 144303, April 2014.

[12] K. M. Hoogeboom-Pota, J. N. Hernandez-Charpaka, X. Gu et al.," A new regime of nanoscale thermal transport: Collective diffusion increases dissipation efficiency," PNAS vol. 112 , pp. 4846–4851, 2015